2022

Enhancing Membrane-Based Air Dehumidification Through Non-Isothermal Operation

Andrew Joseph Fix

James Braun

David M. Warsinger
Purdue University, dwarsing@purdue.edu

Enhancing Membrane-Based Air Dehumidification Through Non-Isothermal Operation

Andrew FIX*, James BRAUN, David WARSINGER

School of Mechanical Engineering, Purdue University
West Lafayette, IN, United States of America
fixa@purdue.edu, jbraun@purdue.edu, dwarsing@purdue.edu

* Corresponding Author

ABSTRACT

Condensation-based air dehumidification has been a major source of inefficiency in air conditioning systems for decades. As global warming progresses and greater populations attain improved thermal comfort, air conditioning energy consumption will grow well past its current benchmark of nearly 2,400 terawatt-hours (10% of the global electricity consumption). Recently, selective membrane-based air dehumidification has gained attention as a promising alternative technology for providing high-efficiency air dehumidification in buildings. Prior work by the authors has presented a system concept, termed the Active Membrane Energy Exchanger (AMX), that exploits clever thermodynamic design to enhance the efficiency of membrane dehumidification and air cooling beyond other proposed membrane-based systems through non-isothermal operation. This work presents the first experimental evaluation of an active non-isothermal membrane-based dehumidification device in the form of an AMX module. The membrane material fabrication and characterization are covered in detail, with particular emphasis on showing the improved membrane permeance to water vapor at cooler air temperatures. The system performance is evaluated while providing simultaneous cooling and membrane dehumidification, showing up to a 6% increase in dehumidification performance, a sensible heat ratio ranging between 0.3-0.7, and an ideal latent coefficient of performance around 2.2. Furthermore, the crossflow tubes (used to carry chilled water) induce an additional 4-8% improvement in dehumidification performance compared to a system without crossflow tubes due to the added air mixing. While prior modeling work has shown the technology can provide up to 60% energy savings through clever system design, the present study provides new insight into additional benefits that were not accounted for in the system models.

1. INTRODUCTION

1.1 Scope and Background

Buildings, both commercial and residential, make up the largest energy consumption sector, constituting a combined 40% of the total primary energy consumption and 76% of the electricity consumption in the United States (Department of Energy, 2015; EIA, 2021). Air cooling and ventilation for buildings is a substantial source of energy consumption. Globally, cooling and ventilation accounts for nearly 10% of the world's electricity consumption (International Energy Agency (IEA), 2018), and dehumidification constitutes up to 80% of the total cooling loads associated with treating outdoor ventilation air in exceptionally hot and humid climates (Harriman et al., 1997). As climate change progresses and as greater populations attain access to thermal comfort technologies, cooling loads, and specifically latent (dehumidification) loads, will grow substantially (Francis, 2021).

Conventional air conditioning systems suffer significant energy penalties associated with condensation dehumidification. Thus, much emphasis has been put into the investigation of separate sensible and latent cooling concepts (Mazzei et al., 2005). Of these options, several alternatives exist, including desiccants (Chua et al., 2018), metal organic frameworks (Cui et al., 2018), and selective membranes (Qu et al., 2018). Selective membranes, which allow water vapor transport but block air, are a particularly promising option. The authors have previously proposed and modeled a novel membrane-based air conditioning system, termed the Active Membrane Energy Exchanger (AMX), which is the first deliberately non-isothermal active membrane dehumidification system concept (A. J. Fix et al., 2021b) and is based on previously proposed system concepts (Claridge & Culp, 2013). Previous work highlighted the theoretical thermodynamic advantages of the design and showed exceptional energy savings over other state-of-the-art systems through modeling (A. Fix et al., 2022; A. J. Fix et al., 2021a). This work, however, presents the first

experimental evaluation of the concept and provides new insight into previously unforeseen advantages of a non-isothermal membrane dehumidification approach.

1.2 Review of Prior System Designs

Membrane-based air dehumidification relies on a difference in water vapor partial pressure across the membrane to draw water vapor out of the humid air stream (Yang et al., 2015). In membrane energy recovery ventilators (M-ERV), a dry air stream and humid air stream are separated by a relatively non-selective membrane, and the natural difference in water vapor partial pressures leads to dehumidification of the humid air stream. In "active" membrane dehumidification systems, a vacuum pump is employed to create a difference in water vapor partial pressure to draw water vapor out of the humid air across the membrane. Vacuum pressures on the order of 1-2 kPa are required to induce this dehumidification, leading to large pressure ratios since the pump must compress the water vapor flow back to atmospheric pressures (Woods, 2014). It is known that "advanced" system designs that reduce the pump pressure ratio are required for membrane systems to achieve substantial energy savings (T. D. Bui, Kum Ja, et al., 2017).

Several "advanced" system designs that can reduce the pump power consumption have been proposed. The first concept is referred to as "vacuum sweep dehumidification," or "VSD," where a portion of the dehumidified air is returned to the vacuum side of the membrane. This enables equally low water vapor partial pressures in the vacuum chamber at higher total pressures, taking advantage of a dry air dilution effect (Scovazzo & Scovazzo, 2012, 2013). The second concept is sub-atmospheric pressure condensation, also known as the Claridge-Culp-Liu cycle, named after the inventors (Claridge, Culp, & Liu, 2019). In this process, water vapor is removed by a membrane and vacuum pump, is compressed slightly (to about 4-5 kPa absolute pressure) such that the pure vapor can be condensed by an ambient temperature condenser (Claridge, Culp, Liu, et al., 2019). The third concept is a "dual-module" membrane dehumidification system, whereby one membrane module removes water vapor from a humid air stream and slightly compresses the water vapor to a second membrane module where the vapor is rejected across the membrane into an exhaust air stream (Claridge & Culp, 2013). Numerous modeling studies have found this last approach to have the greatest potential, closely matched by sub-atmospheric condensation (Labban et al., 2017; Lim et al., 2020).

While each of these "advanced" systems show great promise, there are two major significant limitations of the previous studies: (1) the concepts considered have been limited to isothermal dehumidification and (2) minimal experimental results exist (only VSD has experimental results in the literature). The work presented in this paper provides a fundamental understanding of why non-isothermal operation could be beneficial and provides detailed experimental analyses to support the concept. While the full AMX concept relies on the "dual module" design, this work specifically focuses on analyzing the benefits of the non-isothermal design though experiments on a single module. A depiction of the dual module AMX design is included in the Appendix for reference.

1.3 Review of Membrane Materials

The two most important membrane material properties are water vapor permeance and selectivity. Water vapor permeance describes the ability of the membrane to pass water vapor, and selectivity describes the membrane's ability to block the transport of other gases. The selectivity is often calculated as the ratio of water vapor permeance to N_2 or air permeance. The most common type of membrane for this application is dense polymeric membranes (Woods, 2014). The selective, non-porous layer thickness has a strong impact on permeance and selectivity (Min & Su, 2010). Thus, the aim is to provide very thin selective layers coated on highly porous support substrates to minimize mass transfer resistance for water vapor. These membranes are made by coating a hygroscopic polymer solution onto a highly porous support substrate. The water vapor must first adsorb onto the dense layer and then diffuse through this layer to the opposite, low vapor pressure side of the membrane. This combined process of adsorption and diffusion will prove useful for the non-isothermal approach analyzed in this work. Some top performing polymeric membrane materials reported in the literature include polyvinyl alcohol (PVA) combined with triethylene glycol (T. D. Bui, Wong, et al., 2017), various forms of cellulose acetate (Puspasari et al., 2018), freestanding graphene oxide (Shin et al., 2016), and Pebax 1657 combined with graphene oxide (Akhtar et al., 2017).

The water vapor permeance for most of these membranes displays a clear dependence on both the air temperature and humidity. Generally, water vapor permeance increases for higher relative humidity and lower air temperatures. The temperature dependence stems from the previously mentioned combined process of water vapor adsorption and diffusion. Adsorption generally improves at lower temperatures, while diffusion is generally worse at lower temperatures (D. T. Bui et al., 2016). The net effect for many of these materials, thought not all, is increased water vapor permeance at lower temperatures, which is beneficial for minimizing system size and optimizing effectiveness.

Thus, if warm air must be cooled and dehumidified, it could make sense to cool and dehumidify it at the same time to take advantage of this temperature dependence. Cooling before dehumidifying could be an option but would be limited by the dew point of the air. Dehumidifying and cooling at the same time can enable cooler supply temperatures since the dew point of the air is being reduced by the membranes while also being cooled. Thus, it is necessary to examine this phenomenon in an actual prototype implementation, which is the core contribution of this work.

2. EXPERIMENTAL METHODS AND DESIGN

2.1 Experimental System Design

A test bench that enables the control of air temperature and humidity was developed, and a prototype AMX module was designed, fabricated, and assembled.

Figure 1 shows a schematic of the entire test bench. Compressed air is fed to two mass flow controllers. One air stream remains dry while the other stream is sent to a bubbling device, which brings the air close to saturation (

Figure 1, left). These two air streams are then mixed, and the ratio of flowrates controls the humidity level of the air sent to the experiment. Six feet of aluminum tubing wrapped in controllable heating tape then raises the temperature of the mixed flow for warm air experiments.

The air channel has 8 cooling tubes (3mm OD) running perpendicular to the flow and is between two membranes exposed to vacuum pressures on the opposite sides (

Figure 1, top-right). The air flow channel is approximately 8 cm × 13 cm × 0.635 cm (W×L×H). More details on the geometry of the prototype module can be found in the Appendix. Chilled water is supplied to the cooling tubes by a separate temperature-controlled water recirculator. A vacuum pump pulls a vacuum pressure on the opposite side of each membrane, causing water vapor to transport through the membranes out of the air. The locations of temperature, pressure, and humidity measurements are shown in

Figure 1.

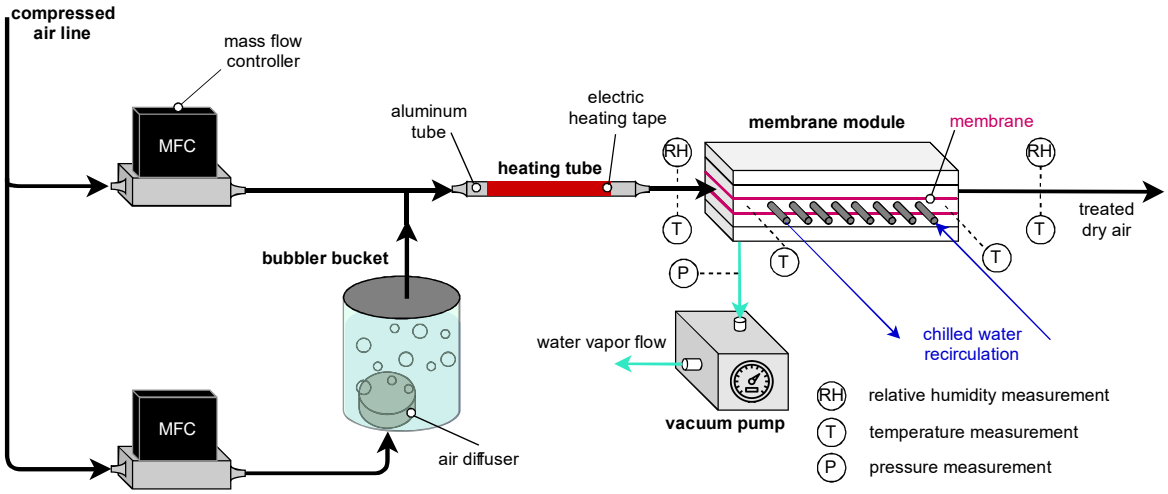

Figure 1. Schematic of the AMX test bench including all sub-components, measurement points, control devices, and membrane module.

2.2 System-Level Experimental Procedures

Results presented in this work are for steady-state operation, and this section provides a general overview of the experimental procedures. System-level performance was characterized for various flowrates, temperatures, and humidity values. For isothermal dehumidification tests, a particular flowrate, temperature, and humidity were chosen. The system settings were adjusted until steady-state conditions were achieved. For non-isothermal experiments (i.e., experiments with the cooling tubes providing sensible cooling), the flowrate, temperature, and humidity were set. The tests then alternated between tests with and without chilled water supply (or in other words, alternated between non-isothermal and isothermal tests). Alternating between tests enabled a fair and accurate comparison of the non-

isothermal performance against the isothermal performance. The non-isothermal tests were run at constant inlet dew point temperatures (or constant inlet absolute humidity) for each dry bulb temperature condition.
Post-processing was carried out using in-house Python codes that incorporate CoolProp (Bell et al., 2014) for humid air calculations. For all system-level experimental tests in this work, each data point was taken 3 times in the same testing session. The standard deviation between these 3 tests was used to quantify the uncertainty. It should be noted that the system performance is sensitive to the membrane properties, small defects, and other setup variances. For this reason, running the same test condition a few days apart with different membranes does not always yield identical results. The trends remained the same but would be shifted up or down. Thus, it can be seen in the results, that most of data was highly repeatable for the given day of testing for each data point, but variance when changing membranes or using the same membranes for several days was noticeable.

2.3 Membrane Fabrication and Characterization
In this work, Pebax 1657 membranes combined with graphene oxide (GO) were used. The fabrication procedures were modified from the original literature that proposed this material combination (Akhtar et al., 2017). The main modification was the use of a porous PVDF substrate instead of the PAN substrate used in the original literature. To summarize the fabrication process, Pebax 1657 was dissolved in a mixture of water/ethanol (30/70 by volume) to form a solution that was 3% Pebax 1657 by weight. A solution of graphene oxide dispersed in water (4 mg/mL) was further diluted to a concentration of 0.18 mg/mL and then combined with the Pebax/water/ethanol solution to create a "GO loading" of 1.5% by weight. The definition of "GO loading" is given by Equation 1 (Akhtar et al., 2017).

$$Load_{GO} = \frac{m_{GO}}{m_{GO} + m_{Pebax}} \tag{1}$$

Here, m_{GO} is the mass of graphene oxide and m_{Pebax} is the mass of Pebax 1657 in the final solution. This combined solution of water, ethanol, Pebax 1657, and graphene oxide was stirred vigorously for 24 hours, followed by 15 minutes of sonication. The solution was then poured into a large container. Supports were cut from a sheet of porous, hydrophobic PVDF with average pore size of 0.22 microns. The sheets were dipped into the solution for 10-15 seconds and then hung to dry between dip coats. The membranes were dipped five times and then allowed to dry at ambient conditions for 24 hours. Finally, they were vacuum dried at 60℃ for an additional 24 hours before use.

The water vapor permeance of the membranes was tested according to the ASTM E96 cup test method (ASTM E96, 2019). Both the "wet cup" and "dry cup" methods were used. In the "wet cup" tests, a cup was filled with distilled water and sealed with a membrane. The surrounding air temperature and humidity were controlled. The change in mass over a given time period was measured and used to calculate the permeance. The "dry cup" method is similar, except the cup was filled with a desiccant. Water vapor transports into the cup, leading to an increase in mass over time. The change in mass is used to calculate the water vapor permeance. Equation 2 details the calculation of the water vapor permeance, β_{H_2O}, for the "wet cup" tests;

$$\beta_{H_2O} = \left(\frac{m_i - m_f}{(1 - RH)P_{sat}At}\right)\left(\frac{1}{MW * 3.35 * 10^{-10}}\right) \tag{2}$$

where m_f is the final measured mass (g), m_i is the initial mass (g), RH is the relative humidity of the surroundings, A is the membrane area (m^2), t is the time (s), MW is the molecular weight of water (g/mol), and the constant in the denominator converts the value to gas permeance units, GPU, which is a common and convenient metric for reporting permeance. The dry cup calculations follow a very similar calculation, simply replacing $(1 - RH)$ with RH and flipping the order of subtraction in the numerator.

The nitrogen permeance testing was carried out according to the ISO 15105 standard (ISO, 2007). Essentially, one side of the membrane was exposed to high pressure nitrogen gas. The other side of the membrane was exposed to a constant volume initially at atmospheric pressure. As nitrogen permeates across the membrane into the constant volume, the pressure of the constant volume increases. This increase in pressure over time is correlated to membrane permeance using Equation 3.

$$\beta_{N_2} = \frac{V_c}{RTAP_h}\frac{dP}{dt}\left(\frac{1}{3.35 * 10^{-10}}\right) \tag{3}$$

Here, V_c is the constant volume of the test cell (L), R is the universal gas constant $\left(\frac{L*Pa}{mol*K}\right)$, T is the gas temperature (K), A is the membrane area (m^2), P_h is the high feed pressure (Pa), and dP/dt is the rate of pressure increase versus time (Pa/s). Figure 2 summarizes the various material characterization tests described above. SEM imaging of the membrane was conducted using the Hitachi-S-4800 field emission machine at the Birck Nanotechnology Center.

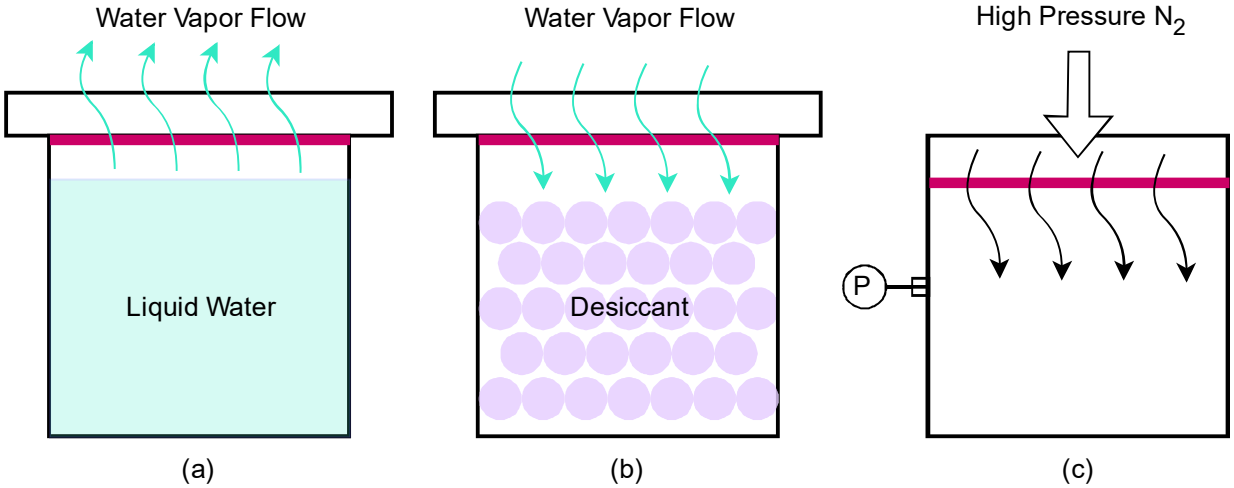

Figure 2. Depiction of the ASTM E96 "wet cup" (a) and "dry cup" (b) methods for determining a material's permeance to water vapor. The ISO 15105 test for determining nitrogen permeance is shown in (c).

3. RESULTS AND DISCUSSION

The results presented in this section include membrane material morphology and properties, the impact of crossflow tubes and simultaneous cooling on the dehumidification performance, and an idealized assessment of the energy consumption. These results present a wholistic understanding of the benefit of non-isothermal membrane dehumidification.

3.1 Membrane Morphology and Characteristics

First, a cross-section view of the membranes incorporated in the prototype system in this work is presented in Figure 3. This image clearly shows the thin, dense layer comprised of Pebax 1657 and GO coated onto the highly porous PVDF substrate. This layer shows excellent uniformity and appears to be less than 1 micrometer thick. This image gives confidence that the fabrication process was successful in providing a thin, dense film without clogging the interior porous structure. Choosing PVDF as a support material likely assists this feature since PVDF is hydrophobic, thus making it difficult for the water-based polymer solution to penetrate beyond the surface during the coating process.

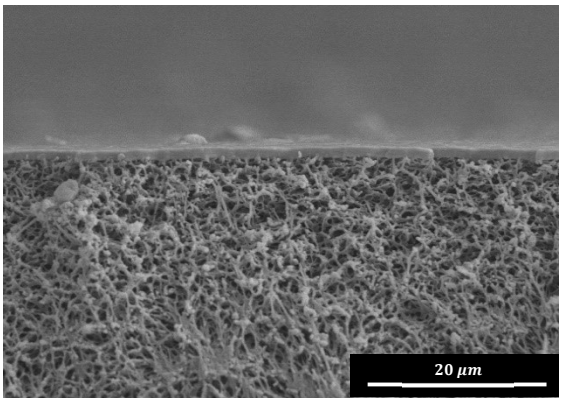

Figure 3. Cross-section SEM image of the dense Pebax 1657 + GO layer coated onto the highly porous PVDF substrate.

Table 1. Summary of the membrane permeance to water vapor, nitrogen gas, and membrane selectivity. Water vapor permeance was tested using the "wet cup" method with the surrounding air at 20℃ and 50% RH.

Parameter	Value
H_2O Vapor Permeance, β_{H_2O}	2576 ± 273 GPU
N_2 Permeance, β_{N_2}	2.32 ± 0.839 GPU
H_2O/N_2 Selectivity	1110

Table 1 shows the average permeance and selectivity values measured at room temperature/humidity conditions. The average value from the wet cup test method is presented since this is the simplest and most common approach presented in the literature. The measured selectivity value is lower than some of the membranes reported in the literature, though it is still acceptably high. Of course, it is also of interest to evaluate the membrane material's permeance dependence on temperature and relative humidity, especially since prior literature did not consider temperature dependence for this material.

Figure 4 shows the water vapor permeance tested using both the wet cup and dry cup methods as a function of temperature and relative humidity. These results show a relatively strong dependence on the air temperature – the permeance at 20℃ is approximately 40% higher than the value at 40℃ for both dry cup tests and nearly 10% higher for the wet cup tests. Thus, there is good reason to believe that non-isothermal dehumidification using these membranes would be beneficial since cooling even a few degrees could provide a significant increase in permeance (improving performance). The difference in 50% RH tests is likely explained by the fact that, in the wet cup analysis, the inside of the test container, where humidity is removed from, is at nearly 100% RH. In the dry cup tests, water vapor is removed from the surrounding air, which is only at 50% RH, and we know permeance increases with increasing humidity.

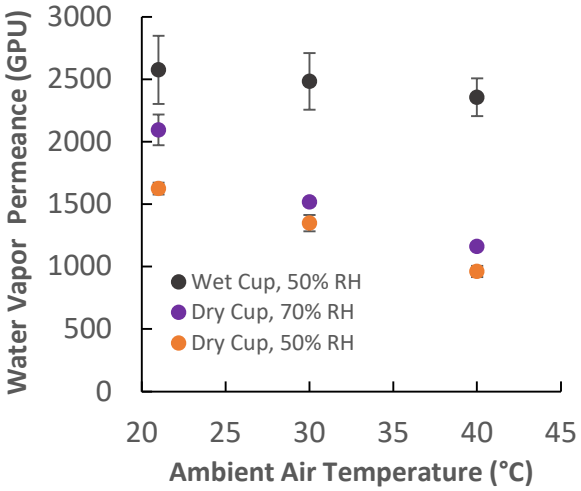

Figure 4. Membrane water vapor permeance as a function of the temperature and relative humidity using both the wet cup and dry cup methods.

3.2 Membrane Module Isothermal Dehumidification Performance

While the ultimate goal of this work is to establish an understanding of the impact of non-isothermal operation on membrane-based air dehumidification, it is first necessary to characterize the dehumidification performance of the prototype AMX module under isothermal conditions (i.e., without cooling tube operation) to establish a baseline for the system performance. Additionally, such an analysis allows straightforward investigation of the dehumidification dependence on the flowrate and relative humidity. The metric that will be used to quantify the dehumidification performance throughout this work is the humidity reduction fraction, defined according to Equation 4.

$$HRF = \frac{\omega_{in} - \omega_{out}}{\omega_{in}} \tag{4}$$

Here, ω represents the humidity ratio in two locations of the experiment: the air channel inlet (in) and the air channel outlet (out). This metric is common in membrane dehumidification data. It can also be useful to define the "latent effectiveness" using the water vapor partial pressures of the flow and vacuum, however this requires separate experimental procedures outside the scope of the present work.

Additionally, in most similar experimental literature, the performance dependence on flow velocity is often reported. Doing so allows greater generalizability of the results for comparison to other prototype systems. The average flow velocity, $\bar{u}_{air}$, is calculated based on the volumetric flowrate and the air channel flow area, according to Equation 5.

$$\bar{u}_{air} = \frac{\dot{V}_{air}}{A_{ch}} = \frac{\dot{V}_{air}}{W * H} \tag{5}$$

Here, $\dot{V}_{air}$ is the volumetric flowrate of air being passed through the module, A_{ch} is the channel flow area, and W and H are the channel width and height, respectively. As can be seen in Figure A1 of the appendix, the air flow enters the air channel through two small tubes, thus the flow velocity immediately upon channel entry will be higher than the calculation provided by Equation 5. Additionally, the perpendicular cooling tubes will have an impact of the flow velocity. However, Equation 5 calculates the velocity based on the simplest geometric dimensions to give insight into average flow velocity with good generalizability. Figure 5 shows the humidity reduction fraction as a function of both flowrate and average flow velocity.

As can be seen in Figure 5, the AMX module performance shows a strong dependence on both the flowrate and the inlet relative humidity, both of which are expected trends. As flowrates increase, the flow moves faster through the module, spending less time in contact with the membranes, and therefore a smaller percentage of the humidity is removed. Additionally, at higher inlet relative humidity values, the water vapor permeance is enhanced, and the concentration gradients induced by the membrane will be stronger, helping minimize concentration polarization.

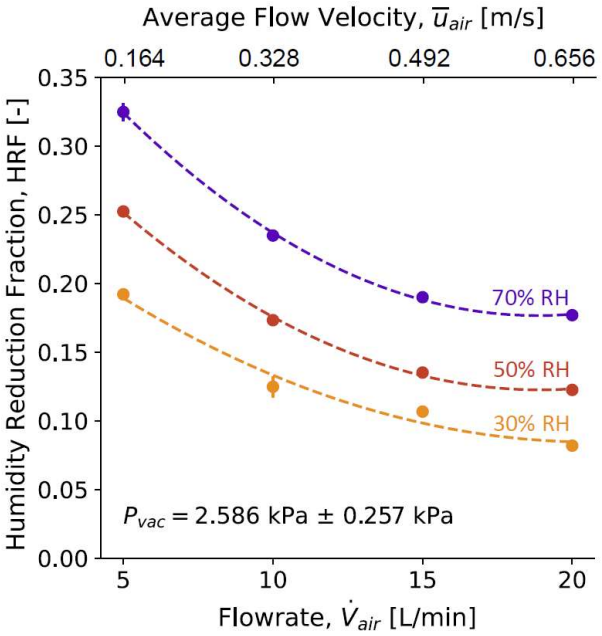

Figure 5. Humidity removal fraction at room temperature as a function of both flowrate and average flow velocity.

It is also useful to understand if the tubes being placed in a crossflow orientation have an impact on the dehumidification performance. To evaluate this, isothermal dehumidification tests were run with and without the tubes installed in the membrane module. The results of this analysis are shown in Figure 6. As can be seen, the dehumidification performance with tubes is, on average, around 4-8% higher than the performance without tubes, suggesting that simply having tubes in the flow enhances the dehumidification performance, even without cooling. This is likely due to the fact that the tubes help disrupt the flow, creating greater mixing and local flow velocities (higher mass transfer coefficients).

3.3 AMX Non-Isothermal Operation Performance

Now comes the core contribution of this work: understanding the impact of non-isothermal operation. The goal is to evaluate whether cooling the air while dehumidifying the air provides any tangible benefit in a real system application, since at the material-level, substantial improvement is observed. Again, this question is investigated by analyzing the system humidity reduction fraction with and without simultaneous cooling. For these particular tests, an inlet dew point temperature of 13°C was maintained across all test conditions (i.e., the inlet absolute humidity was held constant) for a constant flowrate of 10 L/min. For non-isothermal tests, chilled water at 15°C was supplied to the cooling tubes. This choice of cooling tube temperature and inlet dew point temperature ensures no condensation dehumidification can occur, which would skew the results.

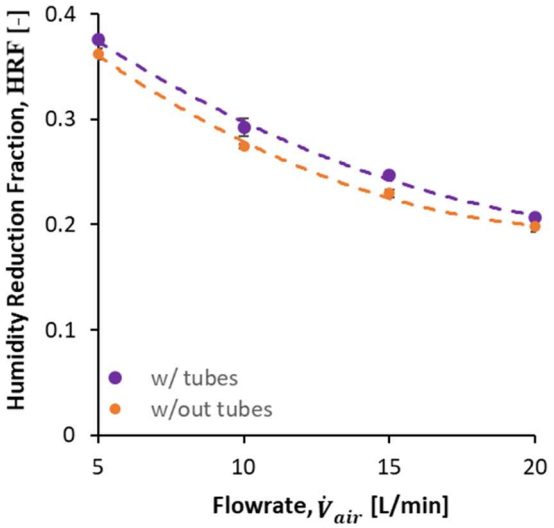

Figure 6. Humidity reduction fraction comparison with and without the tubes installed in the module for an inlet relative humidity of 50% at room temperature.

As can be seen in Figure 7, the results show a somewhat non-intuitive trend in humidity reduction fraction with the inlet air temperature. However, it can be seen that across all test points, dehumidification performance with simultaneous cooling (non-isothermal) achieves equal or better performance, increasing the humidity reduction fraction by as much as 6%.

Looking at Figure 4, we might expect more substantial improvements in humidity reduction fraction since the permeance is strongly dependent on the temperature. However, this lower improvement in humidity reduction fraction can be explained by two factors. First, the sensible heat transfer effectiveness, was usually on the order of 40-50% for these tests such that the average membrane temperature was significantly higher than the coolant flowing through the tubes. For example, at a test air inlet condition of 30°C, the outlet temperature was approximately 22.5°C, with an average air temperature somewhere in between. Therefore, the average temperature that the membrane is exposed to

is only about 4-5℃ cooler than the inlet air temperature. Second, convective resistance plays a significant role in hindering membrane dehumidification. This convective resistance is likely more prominent in an actual prototype system than what the membrane experiences in ASTM E96 cup tests. For both of these reasons, an overall system improvement in *humidity reduction fraction* of 3-6% is quite good and expected.

At this point, it is important to recall that the overall AMX system concept presented in prior modeling literature by the authors has significant thermodynamic benefits. In addition to these thermodynamic benefits for the AMX system, non-isothermal membrane dehumidification fundamentally improves dehumidification performance, irrespective of the system, and should therefore be considered in other advanced membrane dehumidification systems too.

Another interesting metric to present is the sensible heat ratio (SHR). This is a common performance metric in conventional HVAC systems and describes the fraction of sensible heat transfer to the total heat transfer (sensible and latent). It can be calculated according to Equation 6.

$$SHR = \frac{c_p(T_{in} - T_{out})}{h(T_{in},\omega_{in}) - h(T_{out},\omega_{out})} \quad (6)$$

The results, shown in Figure 8, are particularly unique to the AMX technology. Since the cooling tubes are warmer than the dew point temperature, a conventional system operating at similar temperatures would see no dehumidification (SHR=1) and isothermal dehumidification systems would have no sensible cooling (SHR=0). But, the SHR for the AMX can be less than one and non-zero for these conditions. As the inlet air temperature increases, the sensible heat transfer becomes a more significant portion of the total heat removal, evident in the increasing SHR. These results highlight the potential of the AMX as a disruptive technology because of the energy benefits associated with its ability to remove moisture while cooling air with cooling tubes that are above the air dewpoint.

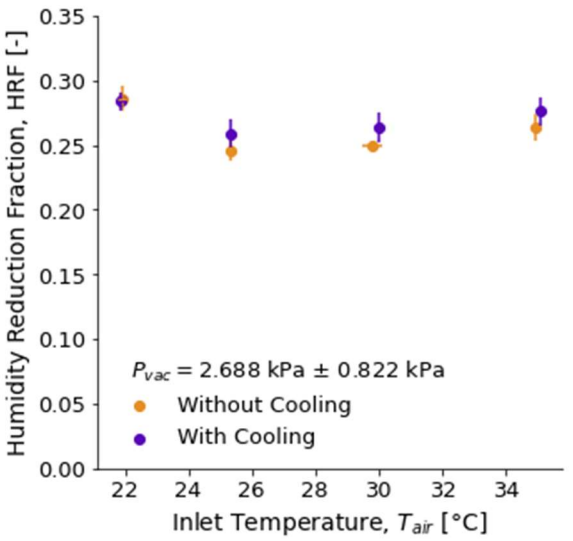

Figure 7. Comparison of the humidity reduction fraction with and without simultaneous cooling provided for a flowrate of 10 L/min and constant inlet dew point temperature of 13℃

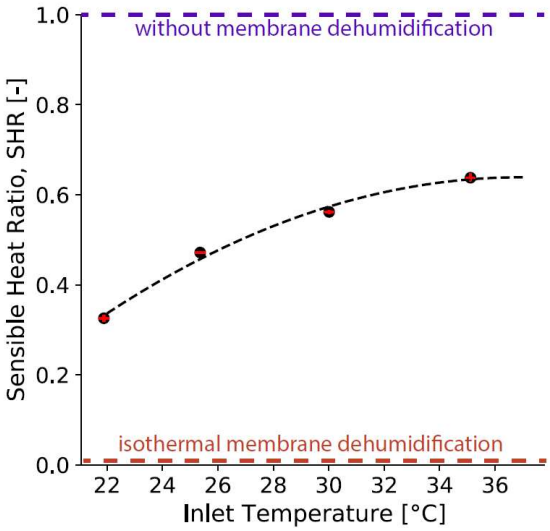

Figure 8. Sensible heat ratio for the Active Membrane Energy Exchanger as a function of the inlet dry bulb temperature for a constant inlet dew point temperature of 13℃ ($\dot{V}_{air}$=10 L/min).

3.4 Latent Coefficient of Performance

The last performance metric that will be discussed is the latent coefficient of performance, which relates the latent heat removed to the power consumption of the vacuum pump. In this work, the vacuum pump was well oversized and therefore consumed a significant amount power compared to the latent heat removal rate, leading to low COPs. This is simply due to the constraints of the overall experiment. Very low vacuum pressures were required, which cannot be achieved by smaller pumps. Plus, pump compatibility with high humidity conditions placed additional limitations on the pump options. For this reason, we instead define the "ideal latent COP," which relates the latent heat of vaporization to the specific energy consumption for an isentropic vacuum pump coupled with a perfect membrane (i.e., only water vapor passes through the membrane). Equation 7 defines this ideal latent COP, $COP_{\mathrm{L,ideal}}$.

$$COP_{\mathrm{L,ideal}} = \frac{h_{fg}}{h_w(P_{atm},\ s = s_{in}) - h_w(P_{vap,vac,i},\ T_{in})} \quad (7)$$

Here, $P_{vap,vac,i}$ is the ideal vacuum vapor partial pressure, meaning the maximum possible vacuum water vapor pressure allowable for the given air flow outlet humidity. For this analysis, we can assume that in an ideal system, the air outlet water vapor partial pressure would be equal to the water vapor partial pressure in the vacuum. Thus, $P_{vap,vac,i}$ is defined according to Equation 8.

$$P_{vap,vac,i} = RH_{outlet} * P_{w,sat} \tag{8}$$

Here, RH_{outlet} is the relative humidity of the outlet and $P_{w,sat}$ is the water vapor saturation pressure at the outlet temperature. Of course, the real system does not operate at this vacuum water vapor partial pressure, as this would imply an effectiveness of 1. However, measuring the water vapor partial pressure under vacuum conditions is challenging, and analyzing the performance in this manner ties all of the data to a unified idealized scenario.

The ideal latent COP is plotted in Figure 9 for the same experimental data points presented in Figure 7. First, the experimental points are shown, and upon first glance, there seems to be some small dependence on temperature. However, when plotting the ideal latent COP as a function of temperature for a constant vacuum vapor partial pressure (shown by the dashed line), the dependence on temperature is rather weak. Instead, the variance between experimental data points is due to the variance in outlet conditions between tests. Interestingly, all of the experimental data points show an outlet water vapor partial pressure (also $P_{vap,vac,i}$) of around 1 kPa (and follow closely with the line).

This plot highlights the fact that more "advanced" system designs that reduce the pump power consumption are required to make the technology competitive, since the real latent COP is much lower than the presented ideal scenario and conventional cooling technologies can have significantly higher COPs. Previous works have shown that pressure ratios on the order of 3-5 are ideal for providing large energy savings and avoiding pump condensation (A. J. Fix et al., 2021a). Nevertheless, the latent COP must be greater than 3-4 in order to compete with conventional vapor compression systems, with COPs in the same range. Reducing the pump/compressor pressure ratio is the key to achieving this, but few or no off the shelf components are optimized for such an application currently.

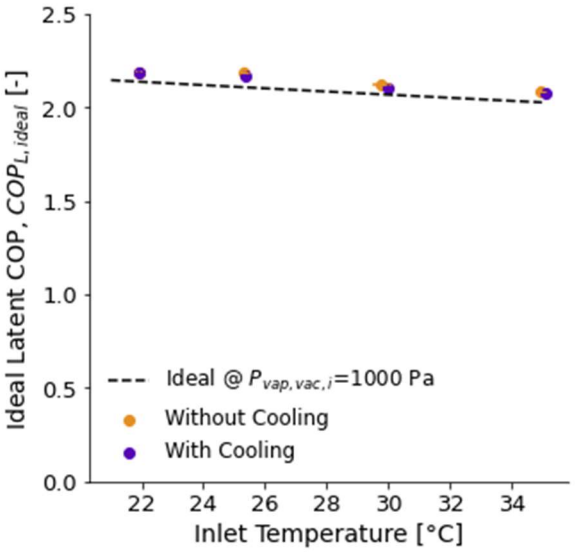

Figure 9. Ideal latent COP as a function of the inlet air temperature for the experimental data.

4. CONCLUSIONS

This work presents the first experimental evaluation of an "Active Membrane Energy Exchanger" prototype module, which is the first membrane-based dehumidification system that seeks to exploit the benefits of non-isothermal dehumidification. On top of the system-level benefits of the approach detailed in prior work by the authors, the present study highlights additional advantages associated with improved performance at cooler air temperatures. The following summarizes the key findings of the work:

- The Pebax 1657 and graphene oxide membranes used in this study showed up to a 40% increase in water vapor permeance when tested at 20℃ compared to 40℃.
- The cross-flow tube configuration, used to cool the air, provided a 4-8% increase in humidity reduction fraction under isothermal conditions. The tubes likely lead to additional pressure drop, but this was not measured in the current study.
- In the benchtop prototype demonstrations, providing simultaneous cooling with membrane dehumidification led to 3-6% improvement in humidity reduction fraction.
- The ideal latent COP was approximately 2.2 for the given test conditions and was very dependent on the ideal vacuum vapor partial pressure. Advanced designs are required to reduce the pump power consumption in order for the AMX to be competitive with conventional cooling technologies.

NOMENCLATURE

AMX	Active Membrane Energy Exchanger
GO	Graphene Oxide
VSD	Vacuum Sweep Dehumidification

A	Area	m^2	$\dot{V}$	Volumetric flow	m^3/s
β	Permeance	GPU	ω	Humidity ratio	kg/kg
c_p	Specific heat	kJ/kg-K	W	Channel width	m
ε	Effectiveness	-			
h	Enthalpy	kJ/kg	**Subscripts**		
H	Channel height	m	H_2O	water	
$\dot{m}$	Mass flowrate	kg/s	in	inlet	
MW	Molecular weight	kg/kmol	out	outlet	
P	Pressure	kPa	vac	vacuum	
R	Gas constant	$\frac{L*Pa}{mol*K}$	vap	vapor	
RH	Relative humidity	-	i	initial	
SHR	Sensible heat ratio	-	f	final	
T	Temperature	℃	sat	saturation	
$\bar{u}$	Flow velocity	m/s	ch	channel	

REFERENCES

Akhtar, F. H., Kumar, M., & Peinemann, K. V. (2017). Pebax®1657/Graphene oxide composite membranes for improved water vapor separation. *Journal of Membrane Science*, *525*, 187–194. https://doi.org/10.1016/j.memsci.2016.10.045

ASTM E96. (2019). *Standard Test Methods for Water Vapor Transmission of Materials*.

Bell, I. H., Wronski, J., Quoilin, S., & Lemort, V. (2014). Pure and pseudo-pure fluid thermophysical property evaluation and the open-source thermophysical property library coolprop. *Industrial and Engineering Chemistry Research*, *53*(6), 2498–2508. https://doi.org/10.1021/ie4033999

Bui, D. T., Nida, A., Ng, K. C., & Chua, K. J. (2016). Water vapor permeation and dehumidification performance of poly(vinyl alcohol)/lithium chloride composite membranes. *Journal of Membrane Science*, *498*, 254–262. https://doi.org/10.1016/j.memsci.2015.10.021

Bui, T. D., Kum Ja, M., Gordon, J. M., Ng, K. C., & Chua, K. J. (2017). A thermodynamic perspective to study energy performance of vacuum-based membrane dehumidification. *Energy*, *132*, 106–115. https://doi.org/10.1016/j.energy.2017.05.075

Bui, T. D., Wong, Y., Thu, K., Oh, S. J., Kum Ja, M., Ng, K. C., Raisul, I., & Chua, K. J. (2017). Effect of hygroscopic materials on water vapor permeation and dehumidification performance of poly(vinyl alcohol) membranes. *Journal of Applied Polymer Science*, *134*, 44765. https://doi.org/10.1002/app.44765

Chua, K. J., Chou, S. K., & Islam, M. R. (2018). On the experimental study of a hybrid dehumidifier comprising membrane and composite desiccants. *Applied Energy*, *220*, 934–943. https://doi.org/10.1016/j.apenergy.2017.12.116

Claridge, D. E., & Culp, C. (2013). *Systems and methods for air dehumidification and cooling with membrane vapor rejection* (Patent No. US 8,500,848 B2).

Claridge, D. E., Culp, C., & Liu, W. (2019). *Systems and methods for multi-stage air dehumidification and cooling* (Patent No. US 2019/0176084).

Claridge, D. E., Culp, C., Liu, W., Pate, M., Haberl, J., Bynum, J., Tanskyi, O., & Schaff, F. (2019). A new approach for drying moist air: The ideal Claridge-Culp-Liu dehumidification process with membrane separation, vacuum compression and sub-atmospheric condensation. *International Journal of Refrigeration*, *101*, 211–217. https://doi.org/10.1016/j.ijrefrig.2019.03.025

Cui, S., Qin, M., Marandi, A., Steggles, V., Wang, S., Feng, X., Nouar, F., & Serre, C. (2018). Metal-Organic Frameworks as advanced moisture sorbents for energy-efficient high temperature cooling. *Scientific Reports*, *8*, 2–10. https://doi.org/10.1038/s41598-018-33704-4

Department of Energy. (2015). Increasing Efficiency of Building Systems and Technologies. In *Quadrennial Technology Review*. https://www.energy.gov/sites/prod/files/2017/03/f34/qtr-2015-chapter5.pdf

EIA. (2021). *Monthly Energy Review* (Issue April).

Fix, A., Braun, J., & Warsinger, D. (2022). Vapor-selective active membrane energy exchanger with mechanical ventilation and indoor air recirculation. *Applied Energy*, *312*, 118768.

Fix, A. J., Braun, J. E., & Warsinger, D. M. (2021a). Vapor-selective active membrane energy exchanger for high efficiency outdoor air treatment. *Applied Energy*, *295*, 116950. https://doi.org/10.1016/j.apenergy.2021.116950

Fix, A. J., Braun, J. E., & Warsinger, D. M. (2021b). *Vapor-Selective Nanostructured Membrane Heat Exchangers for Cooling and Dehumidification* (Patent No. PCT/US2021/019314).

Francis, J. A. (2021). Vapor Storms: More moisture in a warmer atmosphere is fueling intense hurricanes and flooding rains. *Scientific American*, 26–33.

Harriman, L. G., Plager, D., & Kosar, D. (1997). Dehumidification and cooling loads from ventilation air. *ASHRAE Journal*, 37–45. https://doi.org/10.1080/01998595.1999.10530479

International Energy Agency (IEA). (2018). *The Future of Cooling: Opportunities for energy- efficient air conditioning*.

ISO. (2007). *Plastics — Film and sheeting — Determination of gas-transmission rate*. *15105–1*.

Labban, O., Chen, T., Ghoniem, A. F., Lienhard, J. H., & Norford, L. K. (2017). Next-generation HVAC: Prospects for and limitations of desiccant and membrane-based dehumidification and cooling. *Applied Energy*, *200*, 330–346. https://doi.org/10.1016/j.apenergy.2017.05.051

Lim, H., Choi, S., Cho, Y., Kim, S., & Kim, M. (2020). Comparative thermodynamic analysis of membrane-based vacuum air dehumidification systems. *Applied Thermal Engineering*, *179*, 115676. https://doi.org/10.1016/j.applthermaleng.2020.115676

Mazzei, P., Minichiello, F., & Palma, D. (2005). HVAC dehumidification systems for thermal comfort: a critical review. *Applied Thermal Engineering*, *25*, 677–707.

Min, J., & Su, M. (2010). Performance analysis of a membrane-based energy recovery ventilator: Effects of membrane spacing and thickness on the ventilator performance. *Applied Thermal Engineering*, *30*, 991–997. https://doi.org/10.1016/j.applthermaleng.2010.01.010

Puspasari, T., Akhtar, F. H., Ogieglo, W., Alharbi, O., & Peinemann, K. V. (2018). High dehumidification performance of amorphous cellulose composite membranes prepared from trimethylsilyl cellulose. *Journal of Materials Chemistry A*, *6*, 9271–9279. https://doi.org/10.1039/c8ta00350e

Qu, M., Abdelaziz, O., Gao, Z., & Yin, H. (2018). Isothermal membrane-based air dehumidification: A comprehensive review. *Renewable and Sustainable Energy Reviews*, *82*, 4060–4069. https://doi.org/10.1016/j.rser.2017.10.067

Scovazzo, P., & Scovazzo, A. J. (2012). *Dehumidification, dehydration, or drying of uncompressed gases using water selective membranes and a portion of the retentate as a vacuum permeate sweep* (Patent No. WO 2012/151429 Al). World Intellectual Property Organizer.

Scovazzo, P., & Scovazzo, A. J. (2013). Isothermal dehumidification or gas drying using vacuum sweep dehumidification. *Applied Thermal Engineering*, *50*, 225–233. https://doi.org/10.1016/j.applthermaleng.2012.05.019

Shin, Y., Liu, W., Schwenzer, B., Manandhar, S., Chase-Woods, D., Engelhard, M. H., Devanathan, R., Fifield, L. S., Bennett, W. D., Ginovska, B., & Gotthold, D. W. (2016). Graphene oxide membranes with high permeability and selectivity for dehumidification of air. *Carbon*, *106*, 164–170. https://doi.org/10.1016/j.carbon.2016.05.023

Woods, J. (2014). Membrane processes for heating, ventilation, and air conditioning. *Renewable and Sustainable Energy Reviews*, *33*, 290–304. https://doi.org/10.1016/j.rser.2014.01.092

Yang, B., Yuan, W., Gao, F., & Guo, B. (2015). A review of membrane-based air dehumidification. *Indoor and Built Environment*, *24*, 11–26. https://doi.org/10.1177/1420326X13500294

ACKNOWLEDGEMENT

We would like to thank Hamid Fattahi Juybari for his assistance in taking SEM images and the following undergraduate researchers for their contributions to membrane fabrication and characterization, along with some early data acquisition: Songhao Wu, Meghan Thai, Karl Akert, and Hemanth Aroumougam. This work has been financially supported by the Center for High Performance Buildings at Purdue (grant number CHPB-50-2021).

APPENDIX

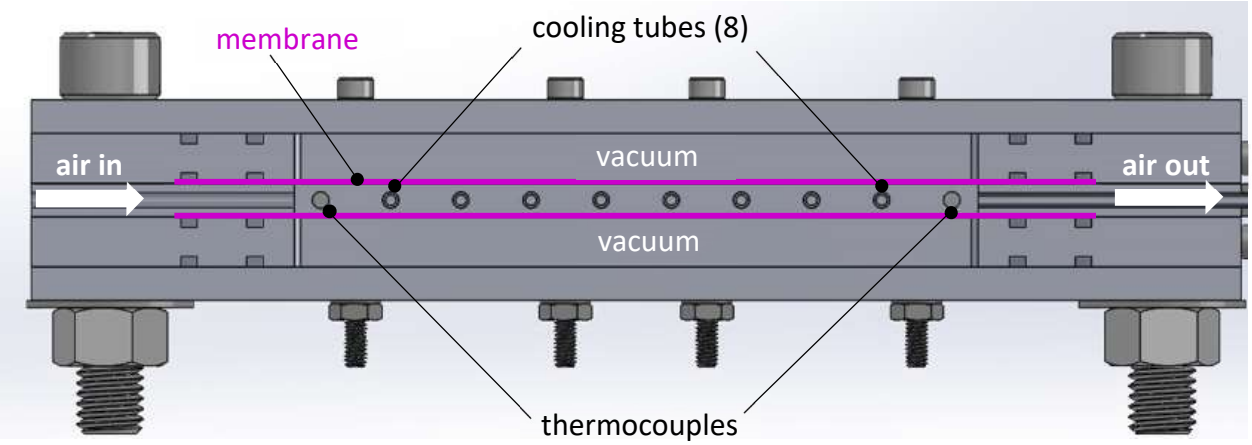

Figure A1. Side cross-section view of the membrane module showing the direction of air flow and the location of cooling tubes and thermocouple probes.

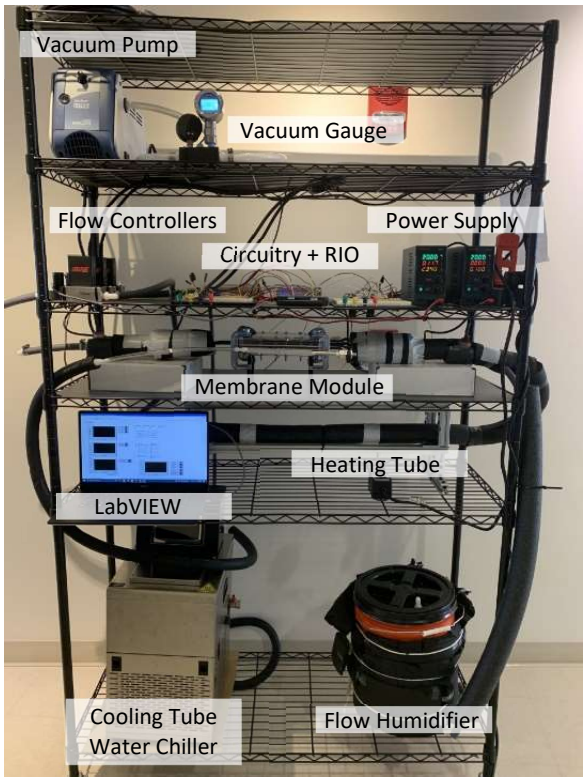

Figure A2. Complete assembly of the experimental test bench used in this study.

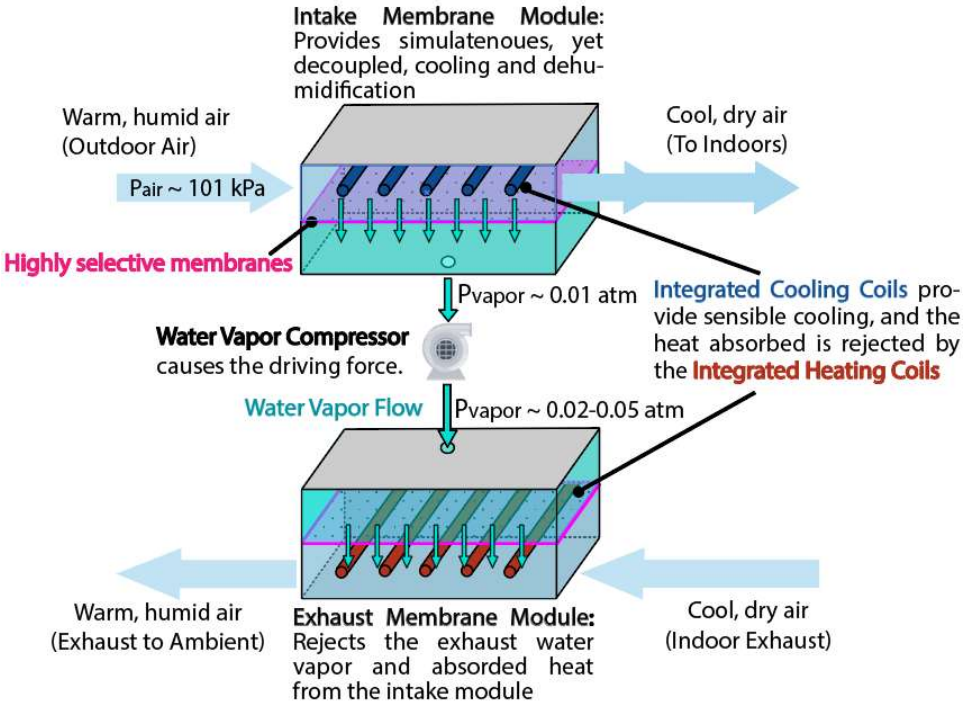

Figure A3. The full, dual-module AMX system concept that removes heat and humidity from the incoming air stream and rejects that heat and humidity to an exhaust air stream in the second membrane module (A. J. Fix et al., 2021a). This work focuses on evaluating the dehumidification performance of a single module connected to a vacuum pump.